Influences of Additives on the Formation of a Solid Electrolyte Interphase on MnO Electrode Studied by Atomic Force Microscopy and Force Spectroscopy

ARTICLE *in* THE JOURNAL OF PHYSICAL CHEMISTRY C · SEPTEMBER 2014

Impact Factor: 4.77 · DOI: 10.1021/jp503953n

9 AUTHORS, INCLUDING:

Rui Wang
Massachusetts Institute of Technology
12 PUBLICATIONS **218** CITATIONS
SEE PROFILE

Weiling Dong
Singapore University of Technology and Design
7 PUBLICATIONS **109** CITATIONS
SEE PROFILE

Wei Lu
Renmin University of China
149 PUBLICATIONS **653** CITATIONS
SEE PROFILE

Hong Li
Chinese Academy of Sciences
277 PUBLICATIONS **10,714** CITATIONS
SEE PROFILE

THE JOURNAL OF PHYSICAL CHEMISTRY C

Article

pubs.acs.org/JPCC

Influences of Additives on the Formation of a Solid Electrolyte Interphase on MnO Electrode Studied by Atomic Force Microscopy and Force Spectroscopy

Jie Zhang,[†,‡] Xiaocheng Yang,[‡] Rui Wang,[§] Weiling Dong,[‡] Wei Lu,*[,‡] Xiaodong Wu,[‡] Xiaoping Wang,[†] Hong Li,[§] and Liwei Chen*[,‡]

[†]Hefei National Laboratory for Physical Sciences at the Microscale, University of Science and Technology of China, Hefei, 230026, P. R. China

[‡]*i*-Lab, Suzhou Institute of Nano-Tech and Nano-Bionics, Chinese Academy of Sciences, Suzhou, Jiangsu 215123, P. R. China

[§]Institute of Physics, Chinese Academy of Sciences, Beijing 100190, P. R. China

Supporting Information

ABSTRACT: The solid electrolyte interphase (SEI) that forms on electrodes largely defines the performances of lithium ion batteries (LIBs), such as cycling performance, shelf life, and safety. Additives in the electrolyte can modify the properties of the SEI and thus efficiently improve the performances of LIBs. However, the effects of additives on the mechanical properties, structure, and stability of the SEI have rarely been studied directly. In this paper, we report the influence of vinylene carbonate (VC) and lithium bis(oxalate)-borate (LiBOB) additives on the mechanical properties of SEI films formed on MnO electrodes using atomic force microscopy (AFM) and force spectroscopy. The results show that the SEI formed from VC additive is thick and soft and partially decomposes upon charging. LiBOB forms thin, stiff, and electrochemically stable SEI films, but the stiff SEI may not be favorable for adapting the volume change of the electrodes. The VC and LiBOB mixed additive combines the advantages of the two components and produces stable SEI with moderate thickness and stiffness. This work also demonstrates that the AFM−force spectroscopy method is effective in investigating the structure and mechanical properties of SEI films.

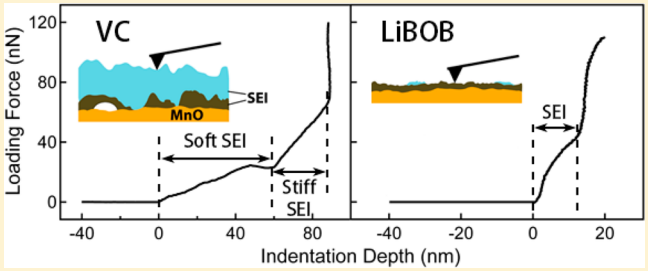

1. INTRODUCTION

The solid electrolyte interphase (SEI) is an ion-conducting and electron-insulating film formed on the electrode surface of lithium-ion batteries (LIB) during charging/discharging cycles. The electrochemical performances of lithium-ion batteries are significantly impacted by the physical and chemical properties of SEI films.[1−3] Many techniques including optical spectroscopy, transmission electron microscopy, and X-ray diffractometry have been used for analyzing the composition and microstructure of SEI films. SEI films have been found to consist of various insoluble organic and inorganic substances (e.g., $ROCO_2Li$,[4] RCOOLi,[5] Li_2CO_3,[6−8] and Li_2O[9,10]) via complicated chemical reactions between the electrolyte and the electrode at different potentials.[11] Therefore, the components of the electrolyte have a major influence on the composition and structure of SEI films, which further impact the battery performance, e.g., cycling performance, Coulombic efficiency, and safety.

Various film-forming additives are formulated into the electrolyte to improve the performance of LIBs to enhance the thermal stability, prevent the cathode from overcharging or dissolution, increase the ion conductance of electrolytes, and facilitate (or suppress) the formation of SEI films on the anode electrode.[3] The effects of additives on the composition and electrochemical properties of SEI films have been studied by spectroscopic and electrochemical methods.[12−16] However, the structure and especially the mechanical properties of SEI films in the presence of additives are rarely known. We have previously established a methodology of investigating SEI film structure and mechanical properties with atomic force microscopy (AFM) and force spectroscopy.[17,18] The results obtained on MnO thin film electrodes demonstrated that the SEI film is distributed on the anode inhomogeneously, and the structure of the SEI agrees with the double-layer model. We suppose that this method can be extended further to study the effect of additives on the structure and mechanical properties of SEI films. In this work, vinylene carbonate (VC) and lithium bis(oxalate)borate (LiBOB) were used as additives to modify the SEI films on MnO film electrodes. The structure, thickness, and mechanical properties of the SEI films were characterized with atomic force spectroscopy and force spectroscopy.

Received: April 23, 2014
Revised: August 8, 2014
Published: August 14, 2014

dx.doi.org/10.1021/jp503953n | *J. Phys. Chem. C* 2014, 118, 20756−20762

2. EXPERIMENTAL METHODS

2.1. Sample Preparation. MnO thin films with a thickness of ~130 nm were prepared on Ti substrates by pulsed laser deposition (PLD).[17] In total, 20 Swagelok-type two-electrode cells were assembled in an argon-filled glovebox (H_2O < 1 ppm, Vigor Co., Suzhou, China) using the MnO films as working electrodes and lithium foils as counter electrodes. The cells were divided into four groups labeled as groups A−D. The composition of the electrolyte used in the cells was 1.0 M $LiPF_6$ dissolved in ethylene carbonate (EC)/propylene carbonate (PC) (1/1, vol) (Novolyte Technologies, Inc. Suzhou, China) with and without additives. The electrolyte of group A was free of additives, but that of groups B−D was with 1% VC, 1% LiBOB, and 0.5% VC + 0.5% LiBOB, respectively. For each group, the cycling processes of five cells were all controlled by an automatic battery tester (Land Co., Wuhan, China) with a constant current density of 6 $\mu A/cm^2$ (~0.11 C). Lithiation and delithation voltage−capacity curves of the MnO electrode without additive, with VC additive, with LiBOB additive, and with VC−LiBOB mixture are presented in Figure S1 (SI). During the first cycle, the discharging processes of four cells were stopped at 0.8, 0.3, 0.1, and 0.01 V, respectively, and the fifth cell was discharged to 0.01 V and then charged back to 3.0 V. The MnO thin film electrodes at different states, hereafter named as Samples A1−A5, B1−B5, C1−C5, and D1−D5, were obtained by dissembling the cells, rinsing with anhydrous dimethyl carbonate (DMC) solvent, and drying under vacuum for further AFM measurements. Noteworthy, although the rinsing and drying process could change the mechanical property of SEI films, the consistent experimental procedure ensures that the data measured from these samples are comparable and the discussion evolving around this data is credible.

2.2. Force Curve Measurements. The rinsed and dried MnO samples were transferred to an Agilent 5500 AFM (Agilent Technologies, Santa Clara, CA) equipped with a homemade glovebox specially designed for oxygen and moisture free AFM environment. Si_3N_4-coated silicon AFM tips (NSC19/Si_3N_4, Mikromasch, Estonia) with a resonant frequency of about 80 kHz and spring constant of about 0.6 nN/nm were used in imaging and force spectroscopy measurements. During the force curve measurement, the tip approaching range was set as 600 nm, and the approaching velocity was 400 nm s^{-1}. For each MnO sample, force curves were collected at more than 300 locations that are randomly distributed on the sample surface. However, some force curves do not contain the information on SEI films (the identification method mentioned below). The proportion of the force curves without SEI signals is shown in Table S1 (SI). Thus, the data points presented in Figures 2−5 may be less than 300.

As shown in Figure 1a, d is the deflection of the cantilever and z is the distance the z-piezo drives the cantilever toward the sample surface. At the point where the tip just comes into contact with the SEI layer, $d = d_0$ and $z = z_0$. Further advancement in z-piezo position (Δz) results in deflection of the cantilever (Δd), and the indentation depth into the SEI layer can be calculated as $\delta = \Delta z - \Delta d$. Since the spring constant of the cantilever can be calibrated accurately, the loading force can thus be calculated and the force curve converted into the indentation curve. Figure 1b shows two typical indentation curves, which are acquired from Samples C4 (left) and B4 (right), respectively. A majority of indentation

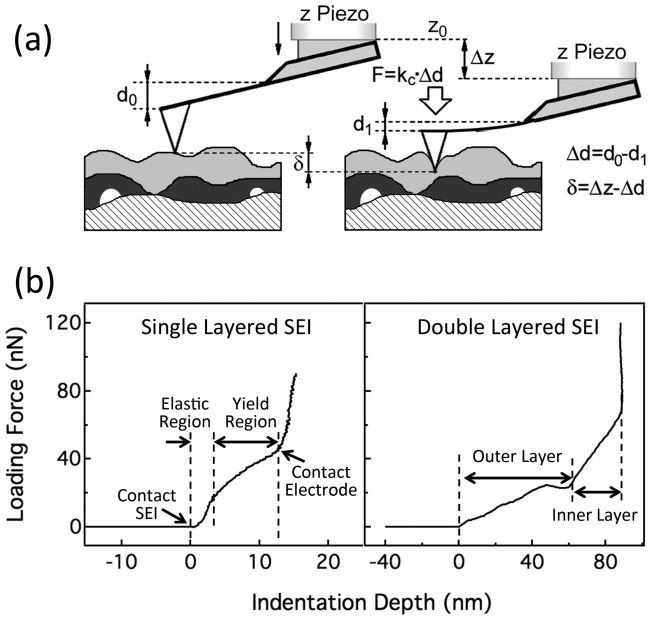

Figure 1. Schematic illustration of AFM−force spectroscopy measurements (a) and typical indentation curves of single layered and double layered SEI (b). When the tip is pushed to the sample beyond the contact point with distance Δz, the tip may be indented into the sample with depth δ, and the cantilever may deflect upward for displacement Δd, where $\Delta z = \delta + \Delta d$.

curves show an initial elastic deformation region followed by a plastic yield region (e.g., the curve on the left in Figure 1b). When the tip first contacts and presses on the SEI, the elastic deformation of the SEI occurs and results in a linear slope in the indentation curve. Upon further indentation, the tip penetrates into the SEI with a relatively small increase in the force, and thus the slope in the indentation curve decreases. After penetrating through the entire SEI, the tip hits the hard solid electrode, and the slope in the indentation curve drastically increases. Importantly, some curves show multilayered structure. For example, the curve on the right in Figure 1b displays two sets of elastic and yield regions before the tip hits the electrode. The thickness and Young's modulus of the SEI film can be quantitatively extracted from the corresponding indentation curves. The thickness is equal to the sum of the indentation depth of elastic and yield regions. The Young's modulus of the SEI film is calculated by fitting the indentation curves with the Sneddon model, which considers the tip as an ideal cone with an infinitesimal tip radius.[19,20] In this paper, the initial linear portion (typically10−30%) of the indentation curve, which can ensure enough data points for fitting, is used to calculate the Young's modulus of SEI films. This range of depth cannot guarantee the absence of influence from the substrate, and thus the modulus values could be affected by the substrate. Considering the substrate is harder than SEI films, the indentation curve should bend upward if the substrate effect is significant. Therefore, only the linear region of the indentation curve is chosen for modulus calculation, to keep the substrate effect within a minor level. Furthermore, since the experimental method and the data processing procedure are all consistent throughout this paper, the trends observed in the paper and the discussion evolving around these data are not affected and are credible.

dx.doi.org/10.1021/jp503953n | J. Phys. Chem. C 2014, 118, 20756−20762

3. RESULTS AND DISCUSSION

3.1. Structural and Mechanical Inhomogeneity of SEI Films. We have established a method using AFM–force spectroscopy to measure the structure, thickness, mechanical property, and the evolution of the SEI on electrodes.[17] On the basis of a detailed analysis on each force curve, the SEI film at a particular location is identified as single-layered (SL), double-layered (DL), or no SEI. Examples of indentation curves with no SEI, SL SEI, and DL SEI are presented in Figures S2, S3, and S4 (Supporting Information), respectively. The SL/DL SEI model can generally be used to describe the SEI films with various thicknesses (thin or thick) and Young's modulus (soft or hard). The thickness and the Young's modulus of each SEI layer can be quantitatively extracted. A plot of the thickness against the modulus is thus a convenient tool to visualize the SEI structure and mechanical properties.

The figures of the SEI layer thickness against the modulus of sample groups A, B, C, and D are plotted in Figures 2, 3, 4, and

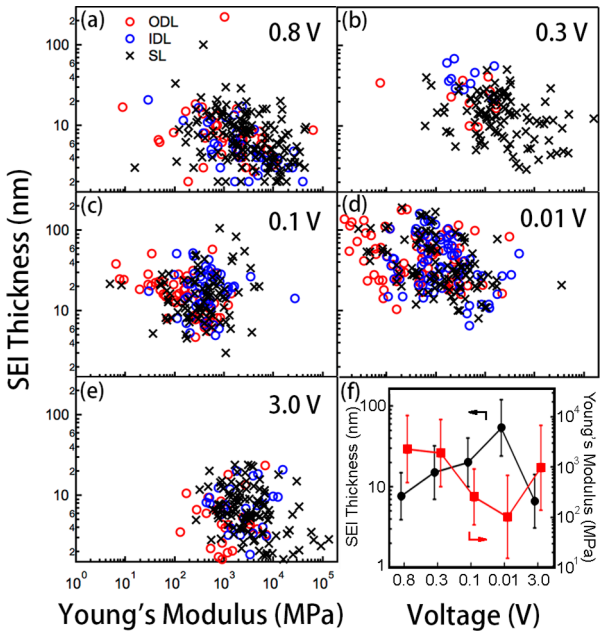

Figure 2. Correlation between SEI thickness and Young's modulus on MnO thin film electrodes in electrolyte without additives at different voltages: 0.8 V (a), 0.3 V (b), 0.1 V (c), 0.01 V (d), and 3.0 V (e). Black crosses are data from SL SEI films; open red circles are data from ODLs; and open blue circles are from IDLs. (f) Geometric average values of SEI thickness and Young's modulus at different voltages.

5, respectively. The black cross, red circle, and blue circle marks correspond to data points from SL, outer layer of double-layered (ODL), and inner layer of double-layered (IDL), respectively. The geometric average thickness and Young's modulus are also plotted in Figures 2f, 3f, 4f, and 5f. The thickness of the SEI varies from a few nanometers to one hundred nanometers, and the Young's modulus varies from 10 MPa to 100 GPa. The observed inhomogeneity in structure, thickness, and mechanical property is consistent with recent results on graphite anodes[21,22] and could be due to the inhomogeneity in the current distribution, surface structure, surface electronic conductivity, and complicated multiple step reactions. Because of the large data dispersion, the geometric average thickness and Young's modulus are used to describe the

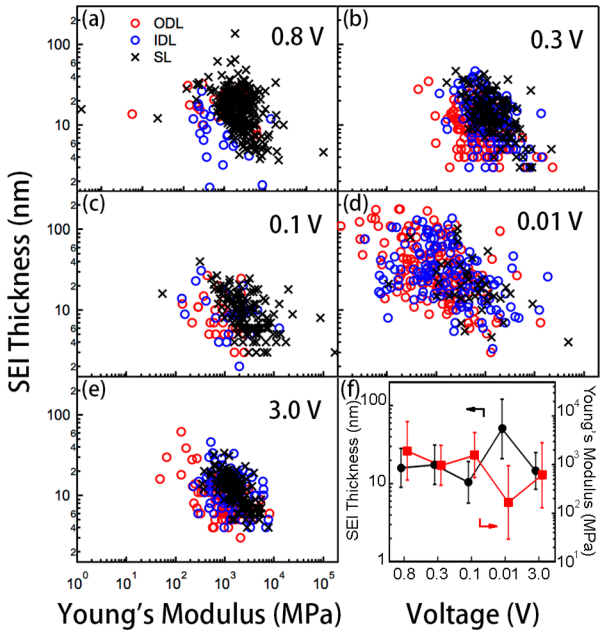

Figure 3. Correlation between SEI thickness and Young's modulus on MnO thin film electrodes in electrolyte with VC as additive at different voltages: 0.8 V (a), 0.3 V (b), 0.1 V (c), 0.01 V (d), and 3.0 V (e). (f) Geometric average values of SEI thickness and Young's modulus at different voltages.

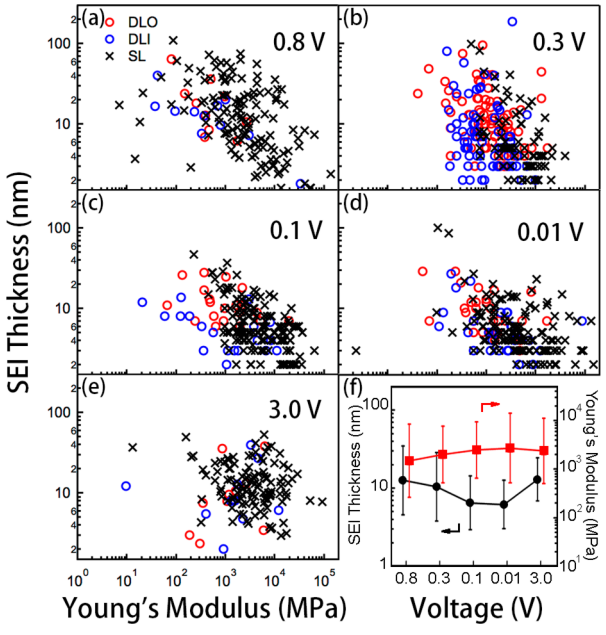

Figure 4. Correlation between SEI thickness and Young's modulus on MnO thin film electrodes in electrolyte with LiBOB as additive at different voltages: 0.8 V (a), 0.3 V (b), 0.1 V (c), 0.01 V (d), and 3.0 V (e). (f) Geometric average values of SEI thickness and Young's modulus at different voltages.

evolution of SEI films in the following discussion. The geometric average thickness was calculated from the thickness of the SL SEI and the entire DL SEI. The geometric average Young's modulus was calculated from the Young's modulus of SL SEI, IDL SEI, and ODL SEI. The inhomogeneity of SEI films is quantified by the geometric standard deviation of thickness and modulus.

dx.doi.org/10.1021/jp503953n | J. Phys. Chem. C 2014, 118, 20756–20762

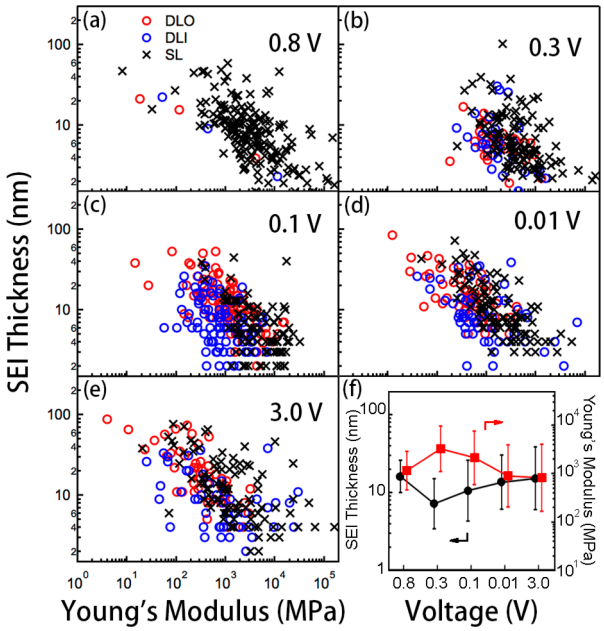

Figure 5. Correlation between SEI thickness and Young's modulus on MnO thin film electrodes in the electrolyte with VC+LiBOB as additive at different voltages: 0.8 V (a), 0.3 V (b), 0.1 V (c), 0.01 V (d), and 3.0 V (e). (f) Geometric average values of SEI thickness and Young's modulus at different voltages.

3.2. Evolution of SEI without Additive. Figure 2a–e shows the thickness vs modulus plot of SEI films formed in the electrolyte without any additive (sample group A) at different voltages. The thickness and Young's modulus of the SEI film increases/decreases with discharging, which are 7.6 nm/2.3 GPa, 15.0 nm/1.9 GPa, 18.1 nm/0.6 GPa, and 45.6 nm/0.1 GPa at 0.8, 0.3, 0.1, and 0.01 V, respectively. The inhomogeneity of the SEI films reaches the maximum at 0.01 V. After the electrode was charged back to 3.0 V, the thickness and the modulus decrease/increase drastically to 6.6 nm/1.0 GPa. During the discharge from 0.8 to 0.01 V, the proportion of DL-SEI increases. These DL-SEI films vanish when charged back to 3.0 V.

Figure 2a–d shows that a large amount of low modulus SEI film is generated during the discharge process from 0.8 to 0.01 V. Especially at 0.01 V, the double-layered SEI film grows significantly, and the Young's modulus of single-/double-layered SEI films becomes much smaller than that at 0.1 V. These results reveal that (1) the predominant components of the inner layer and outer layer of double-layered SEI film could be inorganic and organic substances, respectively, and (2) the 20 nm thick SEI film at 0.1 V is not sufficient to prevent further reduction and decomposition of molecules in electrolyte during discharge from 0.1 to 0.01 V. Since it is difficult to imagine electron conduction through hundreds of nanometers of SEI, the formation of ultrathick SEI films may arise from two possible scenarios: (1) Molecules in the electrolyte could still obtain electrons from the SEI uncovered electrode surface or thin SEI, and reduced further, unsolvable species will diffuse or migrate to deposit on the SEI-covered area. (2) Alternatively, part of the thick SEI films are still electronically conductive. It has been suggested that the contamination of the Mn element on the anode may allow reduction of electrolyte components through thick SEI films.[23]

When the MnO electrode is charged from 0.01 to 3.0 V at the first cycle, the thick SEI films with a small Young's modulus vanishes. This demonstrates that the SEI films generated at 0.1 and 0.01 V are electrochemically unstable. The instability of SEI films on MnO thin film anodes observed by the force spectroscopy is consistent with the transmission electronic microscopy results on MnO powder electrode reported by Zhong et al.[24]

3.3. Evolution of SEI with VC Additive. Figure 3a–e shows the thickness vs modulus plot of SEI films formed in the electrolyte with VC as the additive at different voltages. When the MnO film electrode is discharged to 0.8, 0.3, and 0.1 V, the thickness and modulus of SEI films are relatively stable at 16.0 nm/1.9 GPa, 17.5 nm/1.0 GPa, and 10.5 nm/2.5 GPa, respectively. As the MnO electrode is discharged to 0.01 V, the DL structure becomes dominant, with a thickness of 50 nm and modulus of 0.2 GPa. When the MnO electrode is charged to 3.0 V, most of the thick SEI films formed at 0.01 V disappeared, and the thickness/modulus values return to 14.5 nm/0.6 GPa. It should be noted that the distribution of thickness and modulus measured with VC additive is much narrower than without additive in Figure 2a–e.

Many works have been done to study the effect of VC additive on the formation of SEI films on a graphite anode. The results of these works reveal that the VC additive in PC- and EC-based electrolytes is first reduced to a stable intermediate, then the intermediate is decomposed into free anions and unsaturated alky lithium, which further polymerizes to form lithium-oligomer or polymer.[21,22] The main components of the SEI films formed in the EC-based electrolyte with VC as the additive are $(CHOCO_2Li)_2$, $(CH{=}CHOCO_2Li)_2$, poly VC, and VC oligomer.[25] Because of its high reduction potential (1.0 V vs Li^+/Li), VC forms SEI films before the decomposition of EC during the discharge process.[25] On the basis of these understandings and the larger SEI thickness (16.0 nm) that formed from PC/EC without additive (7.6 nm), we believe that VC should have formed an organic SEI layer over the MnO electrode before discharging to 0.8 V in our experiment. During the discharging process from 0.8 to 0.1 V, organic SEI films formed from the VC additive are further reductively decomposed to generate inorganic SEI films with high Young's modulus. Simultaneously, new SEI with low modulus may also form by partial decomposition of EC and PC on the top of SEI films formed from the VC additive, which leads to double-layered SEI films. Due to the increased electrical resistance of SEI film on the electrode, at 0.01 V a large amount of fresh organic SEI films are generated on the formed SEI films via the predominant single electronic reduction of the electrolyte molecule,[26] resulting in the increase of SEI thickness and the decrease of SEI Young's modulus. After the MnO film electrode is charged from 0.01 V back to 3.0 V, the thickness of SEI films greatly decreases. This could be due to the oxidative decomposition of the organic SEI films formed from EC and PC. However, this oxidative decomposition is not complete because the residual SEI at 3.0 V is 14.5 nm thick and 0.6 GPa in modulus, which is thicker and softer than the 6.6 nm/1.0 GPa SEI formed in bare PC/EC electrolyte without any additive. Therefore, the above results indicate that the VC additive can improve the electrochemical stability of SEI films to a certain level, but the stability is not ideal since partial decomposition of SEI still occurs during charging for a MnO anode.

dx.doi.org/10.1021/jp503953n | J. Phys. Chem. C 2014, 118, 20756–20762

Table 1. Thickness of SEI Films Measured on MnO Thin Film Sample Groups A–D at Different Potentials

potential	0.8 V	0.3 V	0.1 V	0.01 V	3 V
group A (no Additive)	7.6 nm (2.0)	15.0 nm (2.1)	18.1 nm (2.2)	45.6 nm (2.2)	6.6 nm (2.1)
group B (VC additive)	16.0 nm (1.8)	17.5 nm (1.8)	10.5 nm (1.8)	50.3 nm (2.4)	14.5 nm (1.7)
group C (LiBOB additive)	12.6 nm (2.8)	10.4 nm (2.7)	6.5 nm (2.2)	6.2 nm (2.2)	13.0 nm (1.9)
group D (VC + LiBOB additive)	16.2 nm (1.6)	7.2 nm (2.1)	10.6 nm (2.5)	13.6 nm (2.2)	15.3 nm (2.5)

Table 2. Young's Modulus of SL/IDL/ODL Measured on MnO Thin Film Sample Groups A–D under Different Potentials

potential	0.8 V (SL/IDL/ODL)[a]	0.3 V	0.1 V	0.01 V	3 V
group A (no additive)	2.7/2.3/1.1 GPa (4.2/4.5/5.5)	2.0/0.4/0.4 GPa (4.4/2.2/5.0)	0.6/1.3/0.2 GPa (3.9/7.5/4.3)	0.2/0.3/0.04 GPa (7.4/6.2/7.0)	3.8/2.4/1.2 GPa (4.0/2.8/2.8)
group B (VC additive)	2.1/0.9/0.9 GPa (4.1/3.2/4.2)	1.4/1.2/0.7 GPa (2.3/2.3/2.6)	3/1.8/1.3 GPa (4.6/2.8/2.4)	0.5/0.2/0.09 GPa (4.2/5.2/5.1)	1.7/1.2/1.0 GPa (1.9/2.1/3.1)
group C (LiBOB additive)	2.0/0.5/0.3 GPa (8.7/7.0/6.2)	4.5/1.0/1.1 GPa (2.7/2.7/3.2)	1.1/0.2/0.5 GPa (2.8/3.0/3.2)	11.0/3.7/2.0 GPa (9.0/4.4/3.8)	3.4/1.2/1.1 GPa (5.9/6.8/3.3)
group D (VC + LiBOB additive)	1.3/1.1/0.6 GPa (2.0/3.0/2.6)	4.4/1.8/1.7 GPa (3.0/2.6/2.7)	4.5/0.8/1.0 GPa (2.8/2.7/3.4)	2.0/0.9/0.3 GPa (4.3/4.4/6.8)	1.6/0.9/0.3 GPa (6.6/7.2/4.0)

[a](SL/IDL/ODL) stands for thickness of SEI, Young's modulus of SL SEI, IDL SEI, and ODL SEI, respectively.

3.4. Evolution of SEI with LiBOB Additive. Figure 4a–e shows the thickness vs modulus plot of SEI films formed in the electrolyte with LiBOB as the additive at different voltages. Strikingly different from the VC additive and without additive cases, the SEI thickness decreases and the modulus increases as discharging proceeds from 0.8 to 0.01 V. The thickness and modulus are 12.6 nm/1.5 GPa, 10.4 nm/2.0 GPa, 6.5 nm/2.5 GPa, and 6.2 nm/2.7 GPa at 0.8, 0.3, 0.1, and 0.01 V, respectively. When charging back to 3.0 V, the thickness and modulus of SEI films increase/decrease to 13.0 nm/2.4 GPa, which is also different from the VC additive and without additive cases.

The LiBOB additive has two reaction paths to generate the SEI films: (1) the $[BOB]^-$ in LiBOB is reductively decomposed to generate borate and other boron-containing compounds at 1 V;[16,23,24] (2) LiBOB reacts with some components of SEI films such as alkyl lithium or Li_2CO_3 resulting from two-electron reduction of PC and EC, to form a more stable deposition such as semicarbonic acid esters, leading to the increase of electrical resistance in SEI films.[27,28] In our experiments, alky lithium is produced via the reductive decomposition of PC/EC when discharged from 0.8 to 0.1 V, which leads to the increase in proportion of the DL-structure SEI. In the mean time, the LiBOB additive reacts with alky lithium continuously to form dense SEI films containing boron, which consumes the soft organic SEI layer and forms a hard inorganic SEI layer.

As shown in Figure 4f, the thickness/Young's modulus of SEI film decreased/increased with potential decreasing from 0.8 to 0.1 V. This phenomenon may be due to two hypotheses: (1) the thickness of the generated inorganic SEI layer is thinner than that of the consumed organic SEI layer, and (2) the SEI is denser and stiffer at a lower potential, and thus it is harder for the AFM tip to indent and measure the SEI film. When the electrode is discharged to 0.01 V, the thickness and Young's modulus of SEI reach their minimum and maximum, respectively. This implies that the stiff SEI film resulting from the electrolyte with LiBOB additive is highly electrically insulating and can prevent further reduction of the electrolyte by the electrode and thus suppresses the reductive decomposition of electrolyte molecules and the generation of soft organic SEI films, leading to the small proportion of DL SEI films at 0.01 V. These results confirm the hypothesis about the continuous reaction between LiBOB and alky lithium during the discharge process.[27] When charged to 3 V, the SEI thickness increases, and the Young's modulus slightly decreases. These results may be due to the partial decomposition of the inorganic components of SEI films or partial collapse of the SEI film induced by a volume change of the electrode during the charging process from 0.01 to 3 V, and thus the SEI films become less dense. Overall, the LiBOB additive can make the SEI films electrochemically stable, dense, mechanically stiff, and electrically insulating; therefore these SEI films can effectively suppress the decomposition of PC/EC and reduce the irreversible loss of electrolyte. However, the stiff SEI film may not be ideal for accommodating the volume changes of the electrode in cycling.

3.5. Evolution of SEI with VC + LiBOB Additive. As mentioned above, SEI formed by the VC additive contains more organic substances, which may render SEI films more flexible and more accommodative for the volume change of electrode materials during the charging/discharging cycle, but it is electrochemically unstable and decomposes at high voltage. On the other hand, SEI formed by LiBOB additive is denser, more stable, and electrically insulating, which can effectively prevent the continuous decomposition of PC/EC electrolyte, but mechanically more stiff and may not be ideal for preserving the structure against electrode volume change in cycling. To further optimize the SEI, we add the VC + LiBOB mixture into the PC/EC electrolyte as an additive to combine the advantage of both additives (Figure 5). Figure 5a–e shows the thickness vs Young's modulus plot of SEI films formed in the electrolyte with VC + LiBOB mixed additives at different voltages. The SEI films resulting from mixed additives show relative stable thickness and modulus during the discharge/charge cycle: 16.2 nm/1.2 GPa, 7.2 nm/3.3 GPa, 10.6 nm/2.1 GPa, 13.6 nm/0.9 GPa, and 15.3 nm/0.8 GPa at 0.8, 0.3, 0.1, 0.01, and 3.0 V, respectively. The plots in Figure 5a–e also show a common trend that harder SEI films have narrow thickness distribution, while softer SEI films have broader thickness distribution.

For understanding the unique properties of the SEI films formed with VC + LiBOB mixed additive (Group D), we analyze the geometric average and geometric standard deviation (the value in parentheses) of thickness (Table 1) and Young's modulus of SL/ISL/ODL SEI films (Table 2) on sample groups A–D at different potentials.

dx.doi.org/10.1021/jp503953n | J. Phys. Chem. C 2014, 118, 20756–20762

Under 0.8 V, the SEI films formed with VC + LiBOB (Group D) exhibit thickness and Young's modulus (16.0 nm/1.3/1.1/0.6 GPa) very similar to that from VC only (16.0 nm/2.1/0.9/0.9 GPa in Group B). This implies that VC decomposes at 0.8 V, and LiBOB does not react with the reductive product of VC. When discharged to 0.3 V, LiBOB reacts with the VC decomposition product to form thin and stiff films. These SEI films may be less electronic insulating than SEI from LiBOB only; therefore, soft organic SEI films can be formed on the surface when further discharged to 0.1 and 0.01 V. When charged back to 3 V, SEI from VC + LiBOB shows the best stability. Overall, the SEI film formed from the electrolyte with VC + LiBOB mixed additive is electrochemically more stable and electrically more insulating than that formed from the electrolyte with VC additive and mechanically more flexible than that formed from the electrolyte with LiBOB additive. On the basis of the force spectroscopy characterization, we believe the mixed additives are more suitable than each individual additive for practical application in MnO electrodes.

3.6. Bubbles in SEI. During the analyzing of force spectra, we also found some force curves representing the existence of bubbles in SEI. Figure 6 shows a typical force curve when a tip

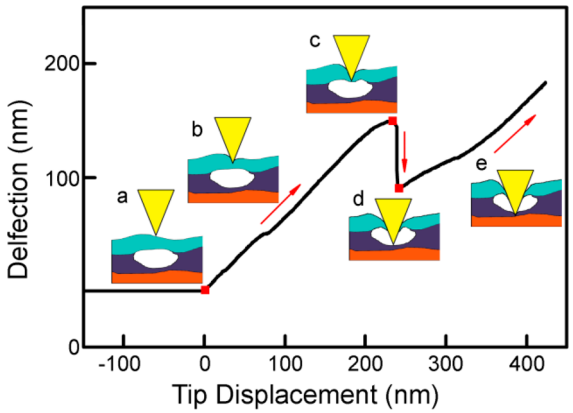

Figure 6. Schematic illustration and typical force curve when the AFM tip indents into a nanobubble.

indents into SEI with possible bubble structure. From point c to d, the deflection signal decreases drastically for about 60 nm, which means there could be a bubble with height of 60 nm within the SEI film. When the tip hits the bottom of the bubble, the cantilever bends up again as the tip moves down. It needs to be noted that such bubble structures can be only found in the force spectra collected from cell discharging to 0.01 V with no additive and with VC additive, and the SEI formed without additives shows more and larger bubbles (Figure S5 presents more force curves of the SEI films containing bubbles in the Supporting Information). We speculate this is because either the bubble (gas) formation may be related with specific chemistry or, more likely, gas bubbles cannot be retained in thin SEI films.

4. CONCLUSION

The structure, thickness, and mechanical properties of SEI formed on MnO film electrodes with various additives were studied using the atomic force microscopy and force spectroscopy method. The structure and property of the SEI film are highly inhomogeneous and change dynamically under different cycling states and when different additives are used. In the absence of additives in the PC/EC/$LiPF_6$ electrolyte, a large quality of soft SEI films was formed on MnO film when the electrode was deeply discharged. These soft SEI films were electrochemically unstable and decomposed after charging to 3.0 V. When VC was added in the electrolyte as additive, the stability was improved but the SEI still decomposed partially upon charging. The LiBOB additive significantly improves the electrochemical stability of the SEI and prevents electrolyte loss in cycling, but its drawback is that the SEI formed is mechanically highly stiff. Interestingly, mixed VC and LiBOB additives produce SEI films with combined advantages of the two components and thus could be best suited for protecting MnO anodes in practical applications. Our investigations indicate further that force spectroscopy is suitable to study complicated SEI and provides unique information.

■ ASSOCIATED CONTENT

Ⓢ Supporting Information

Voltage−capacity curves for lithiation and delithation of MnO electrodes in different electrolytes, representative indentation curves showing no SEI, single-layered SEI and double-layered SEI, the proportion of the force curves without SEI signals, and the force curves of the SEI containing bubble. This material is available free of charge via the Internet at http://pubs.acs.org.

■ AUTHOR INFORMATION

Corresponding Authors

*Wei Lu. Phone: +86-512-6287-2675. E-mail: wlu2008@sinano.ac.cn.

*Liwei Chen. Phone: +86-512-6287-2655. E-mail: lwchen2008@sinano.ac.cn.

Notes

The authors declare no competing financial interest.

■ ACKNOWLEDGMENTS

This project is supported by the "Strategic Priority Research Program" of the CAS, Grant No. XDA09010600, the National Basic Research Program of China (2010CB934700), the National Natural Science Foundation of China (Nos. 21273273 and 21103222), and the Sci. & Tech. Project of Suzhou (ZXJ2012002). W.L. thanks the Funding of Creative Young Scientists, CAS. L.C. acknowledges the support from Jiangsu Provincial Natural Science Foundation (Grant No. BK20130006). We thank Dr. Micah Glaz for checking the writing of this paper.

■ REFERENCES

(1) Aurbach, D. Review of Selected Electrode-Solution Interactions Which Determine the Performance of Li and Li Ion Batteries. *J. Power Sources* **2000**, *89*, 206−218.

(2) Goodenough, J. B.; Kim, Y. Challenges for Rechargeable Li Batteries. *Chem. Mater.* **2010**, *22*, 587−603.

(3) Zhang, S. S. A Review on Electrolyte Additives for Lithium-Ion Batteries. *J. Power Sources* **2006**, *162*, 1379−1394.

(4) Aurbach, D.; Markovsky, B.; Shechter, A.; EinEli, Y.; Cohen, H. A Comparative Study of Synthetic Graphite and Li Electrodes in Electrolyte Solutions Based on Ethylene Carbonate Dimethyl Carbonate Mixtures. *J. Electrochem. Soc.* **1996**, *143*, 3809−3820.

(5) Zhuang, G. R. V.; Ross, P. N. Analysis of the Chemical Composition of the Passive Film on Li-Ion Battery Anodes Using Attentuated Total Reflection Infrared Spectroscopy. *Electrochem. Solid-State Lett.* **2003**, *6*, A136−A139.

(6) Aurbach, D.; Gofer, Y.; Langzam, J. The Correlation between Surface-Chemistry, Surface-Morphology, and Cycling Efficiency of

Lithium Electrodes in a Few Polar Aprotic Systems. *J. Electrochem. Soc.* **1989**, *136*, 3198−3205.
(7) Andersson, A. M.; Henningson, A.; Siegbahn, H.; Jansson, U.; Edstrom, K. Electrochemically Lithiated Graphite Characterised by Photoelectron Spectroscopy. *J. Power Sources* **2003**, *119*, 522−527.
(8) Tsubouchi, S.; Domi, Y.; Doi, T.; Ochida, M.; Nakagawa, H.; Yamanaka, T.; Abe, T.; Ogumi, Z. Spectroscopic Characterization of Surface Films Formed on Edge Plane Graphite in Ethylene Carbonate-Based Electrolytes Containing Film-Forming Additives. *J. Electrochem. Soc.* **2012**, *159*, A1786−A1790.
(9) Aurbach, D.; Levi, M. D.; Levi, E.; Schechter, A. Failure and Stabilization Mechanisms of Graphite Electrodes. *J. Phys. Chem. B* **1997**, *101*, 2195−2206.
(10) Edstrom, K.; Herstedt, M.; Abraham, D. P. A New Look at the Solid Electrolyte Interphase on Graphite Anodes in Li-Ion Batteries. *J. Power Sources* **2006**, *153*, 380−384.
(11) Peled, E.; Golodnitsky, D.; Ardel, G. Advanced Model for Solid Electrolyte Interphase Electrodes in Liquid and Polymer Electrolytes. *J. Electrochem. Soc.* **1997**, *144*, L208−L210.
(12) Aurbach, D.; Gamolsky, K.; Markovsky, B.; Gofer, Y.; Schmidt, M.; Heider, U. On the Use of Vinylene Carbonate (Vc) Electrolyte Solutions for Li-Ion as an Additive to Batteries. *Electrochim. Acta* **2002**, *47*, 1423−1439.
(13) Xu, K.; Lee, U.; Zhang, S. S.; Jow, T. R. Graphite/Electrolyte Interface Formed in Libob-Based Electrolytes - Ii. Potential Dependence of Surface Chemistry on Graphitic Anodes. *J. Electrochem. Soc.* **2004**, *151*, A2106−A2112.
(14) Xu, K.; Zhang, S. S.; Jow, R. Electrochemical Impedance Study of Graphite/Electrolyte Interface Formed in Libob/Pc Electrolyte. *J. Power Sources* **2005**, *143*, 197−202.
(15) Choi, N. S.; Yew, K. H.; Lee, K. Y.; Sung, M.; Kim, H.; Kim, S. S. Effect of Fluoroethylene Carbonate Additive on Interfacial Properties of Silicon Thin-Film Electrode. *J. Power Sources* **2006**, *161*, 1254−1259.
(16) Ochida, M.; Domi, Y.; Doi, T.; Tsubouchi, S.; Nakagawa, H.; Yamanaka, T.; Abe, T.; Ogumi, Z. Influence of Manganese Dissolution on the Degradation of Surface Films on Edge Plane Graphite Negative-Electrodes in Lithium-Ion Batteries. *J. Electrochem. Soc.* **2012**, *159*, A961−A966.
(17) Zhang, J.; Wang, R.; Yang, X. C.; Lu, W.; Wu, X. D.; Wang, X. P.; Li, H.; Chen, L. W. Direct Observation of Inhomogeneous Solid Electrolyte Interphase on Mno Anode with Atomic Force Microscopy and Spectroscopy. *Nano Lett.* **2012**, *12*, 2153−2157.
(18) Weadock, N.; Varongchayakul, N.; Wan, J.; Lee, S.; Seog, J.; Hu, L. Determination of Mechanical Properties of the Sei in Sodium Ion Batteries Via Colloidal Probe Microscopy. *Nano Energy* **2013**, *2*, 713−719.
(19) Sneddon, I. N. The Relation between Load and Penetration in the Axisymmetric Boussinesq Problem for a Punch of Arbitrary Profile. *Int. J. Eng. Sci.* **1965**, *3*, 47−57.
(20) Domke, J.; Radmacher, M. Measuring the Elastic Properties of Thin Polymer Films with the Atomic Force Microscope. *Langmuir* **1998**, *14*, 3320−3325.
(21) Domi, Y.; Ochida, M.; Tsubouchi, S.; Nakagawa, H.; Yamanaka, T.; Doi, T.; Abe, T.; Ogumia, Z. Electrochemical Afm Observation of the Hopg Edge Plane in Ethylene Carbonate-Based Electrolytes Containing Film-Forming Additives. *J. Electrochem. Soc.* **2012**, *159*, A1292−A1297.
(22) Cresce, A. v.; Russell, S. M.; Baker, D. R.; Gaskell, K. J.; Xu, K. In Situ and Quantitative Characterization of Solid Electrolyte Interphases. *Nano Lett.* **2014**, *14*, 1405−1412.
(23) Delacourt, C.; Kwong, A.; Liu, X.; Qiao, R.; Yang, W. L.; Lu, P.; Harris, S. J.; Srinivasan, V. Effect of Manganese Contamination on the Solid-Electrolyte-Interphase Properties in Li-Ion Batteries. *J. Electrochem. Soc.* **2013**, *160*, A1099−A1107.
(24) Zhong, K. F.; Xia, X.; Zhang, B.; Li, H.; Wang, Z. X.; Chen, L. Q. Mno Powder as Anode Active Materials for Lithium Ion Batteries. *J. Power Sources* **2010**, *195*, 3300−3308.
(25) Ota, H.; Sakata, Y.; Inoue, A.; Yamaguchi, S. Analysis of Vinylene Carbonate Derived Sei Layers on Graphite Anode. *J. Electrochem. Soc.* **2004**, *151*, A1659−A1669.
(26) Peled, E.; Golodnttsky, D.; Ardel, G.; Menachem, C.; Bar Tow, D.; Eshkenazy, V. The Role of Sei in Lithium and Lithium Ion Batteries. *MRS Proc.* **1995**, *393*, 209.
(27) Zhang, S. S.; Xu, K.; Jow, T. R. Enhanced Performance of Natural Graphite in Li-Ion Battery by Oxalatoborate Coating. *J. Power Sources* **2004**, *129*, 275−279.
(28) Xu, K.; Lee, U.; Zhang, S. S.; Wood, M.; Jow, T. R. Chemical Analysis of Graphite/Electrolyte Interface Formed in Libob-Based Electrolytes. *Electrochem. Solid-State Lett.* **2003**, *6*, A144−A148.